Experimental investigation of dynamic mixed-mode fracture initiation

John M. Lambros, James J. Mason, Ares J. Rosakis

John M. Lambros, James J. Mason, Ares J. Rosakis, "Experimental investigation of dynamic mixed-mode fracture initiation," Proc. SPIE 1554, Second International Conference on Photomechanics and Speckle Metrology, (1 December 1991); doi: 10.1117/12.49481

SPIE.

Event: San Diego, '91, 1991, San Diego, CA, United States

Experimental Investigation of Dynamic Mixed-Mode Fracture Initiation

J. Lambros, J.J. Mason and A.J. Rosakis

Graduate Aeronautical Laboratories
California Institute of Technology
Pasadena, CA 91125

Abstract

The use of a coherent gradient sensing (CGS) apparatus is explored in dynamic fracture mechanics investigations. The ability of the method to accurately quantify mixed-mode crack tip deformation fields is tested under dynamic loading conditions. The specimen geometry and loading follow that of Lee and Freund[1,2] who give the theoretical and numerical mixed mode K values as a function of time for the testing conditions. The CGS system's measurements of K_I and K_{II} are compared with the predicted results, and good agreement is found.

1. Introduction

The full-field method known as CGS,[3,4] is investigated here for the measurement of mixed-mode, dynamic crack tip deformation fields under plane stress conditions in optically transparent, non-birefringent materials. The Coherent Gradient Sensor is a lateral shearing interferometer utilizing two identical line gratings. The set-up was first proposed for measuring lens abberations,[5,6] but, until recently, other possible applications of the CGS interferometer have been overlooked. When used in fracture mechanics the method gives real time measurements of the in-plane stress gradients for transparent materials or the in-plane gradients of the out-of-plane displacements for opaque materials. With data taken at a wide range of points near the crack tip, it is possible for the CGS method both to show whether or not the stress field at a crack tip is well described by the dominant ($r^{-\frac{1}{2}}$) singular term of the asymptotic expansion (K-dominance) and to find accurate values of K_I and K_{II}, the stress intensity factors.

Tippur et. al.[3,4] have demonstrated the accuracy of the CGS statically for mode I loading, however, its accuracy in dynamic investigations, including dynamic mixed-mode loading, has not been reported.

An analysis of the loading geometry shown in Figure 1b by Lee and Freund[1,2] shows that both modes of deformation, mode I and mode II, can be expected for such a loading geometry.

Apart from the dominant K_{II}, a small negative K_I is also predicted. In this study it is desired to establish the ability of CGS to accurately measure the dynamic, mixed-mode stress intensity factors by comparing experimental results with the solution of Lee and Freund. Also, it is realized that a positive agreement of the measurements of the CGS system with the Lee and Freund solution will confirm the validity of that solution.

2. Theoretical Development

2.1 Analytical Model

One side of an elastic, half-space containing an edge crack is loaded dynamically by some prescribed velocity, $v(t)$. (See Figure 1b.) An elastic plane strain solution to this problem is reported[1,2] for a step input velocity, $v(\tau) = v_o H(\tau)$. For this study, the analysis was adjusted to reflect a plane stress field.

The normalization factor, K', for the stress intensity factors is given by

$$K' = \begin{cases} \sqrt{\frac{l}{\pi}} \frac{E v_o}{2 c_d^{pl-\sigma}} & \text{for plane stress} \\ \sqrt{\frac{l}{\pi}} \frac{E v_o}{2 c_d^{pl-\epsilon} (1-\nu^2)} & \text{for plane strain} \end{cases} \tag{1}$$

The time axis is normalized by the characteristic time, $l/c_d^{pl-\sigma}$ where $c_d^{pl-\sigma}$ is the plane stress dilatational wave speed, and l is the crack length. The results of the plane stress calculations for the model material, PMMA ($\nu = .35$), for both mode I and mode II stress intensity factors are shown in Figures 7a and 7b, respectively.

Most of the qualitative features of the curves in these figures can be explained. Upon impact a plane compressive wave is generated. It is followed by cylindrical unloading waves generated at the corners of the impact area. The compressive wave gives rise to K_{II}. The existence of the unloading wave makes the increase in K_{II} progressively more gradual and forces the crack faces to close, thus causing a smaller, but significant, negative K_I. As can be seen in Figures 7a and 7b there exist three regions in the solution. These correspond to the arrivals at the crack tip of the first dilatational, shear and Rayleigh waves, respectively. The solution is valid up to $c_d t/l = 3$, which corresponds to the arrival of a second dilatational wave that is reflected from the impact surface.

2.2 The Method of CGS

In contrast to Tippur et.al.,[3,4] the theoretical development of CGS shown here follows the more traditional approach of Murty[7] for lateral shearing interferometers. The two approaches are equivalent; the same assumptions are made and the same governing equations result. It is hoped that the more traditional development will result in an easier understanding of the method. A schematic of the set-up is shown in Figure 2. A coherent, collimated laser beam, 50

mm in diameter, passes through a notched transparent specimen. After exiting from the deformed specimen, the beam falls upon the first of two identical diffraction gratings (40 lines/mm). The primary grating splits the beam into a direct beam and numerous diffraction orders. For the sake of brevity, only the first diffraction orders (± 1) and the direct beam are considered. The second diffraction grating diffracts both the direct beam and the first diffraction orders into three beams each, giving a total of nine beams behind the second grating. Of these nine beams the (0,$\pm$1) and the ($\pm$1,0) orders are parallel—as can be seen in Figure 3.

An on-line spatial filter is used to isolate one of the two pairs of parallel beams. A lens is placed a distance equal to its focal length behind the secondary grating as in Figure 2. The Fourier Transform of the intensity distribution at the second grating is observed in the back-focal plane of the lens where an aperture is placed on either the +1 or -1 diffraction order spot. The aperture filters all but the two desired parallel beams from the wavefront. Another lens is placed at a distance equal to its focal length behind the aperture to invert the Fourier transformation.

It is assumed that the wave front before the first grating is approximately planar with some phase difference, $\delta S(x_1, x_2)$. Deviations of the propagation direction from the optical axis are neglected. Thus, the two gratings shift one beam with respect to the other by a distance

$$\epsilon = \Delta tan\theta \approx \Delta\theta \tag{2}$$

where Δ is the separation between the gratings, see Figure 2, and θ is the angle of diffraction (assumed small), given here by

$$\theta = sin^{-1}\frac{\lambda}{p} \approx \frac{\lambda}{p} . \tag{3}$$

λ is the wavelength of the illumination, and p is the pitch of gratings.

The two parallel, sheared wavefronts constructively interfere at a point if their difference in phase is an integer multiple of the wavelength, i.e. if

$$\delta S(x_1 + \epsilon, x_2) - \delta S(x_1, x_2) = m\lambda . \tag{4a}$$

where m is called "the fringe order." Dividing this equation by ϵ gives

$$\frac{\delta S(x_1 + \epsilon, x_2) - \delta S(x_1, x_2)}{\epsilon} = \frac{m\lambda}{\epsilon} , \tag{4b}$$

which, for sufficiently small ϵ, may be approximated by

$$\frac{\partial(\delta S(x_1, x_2))}{\partial x_\alpha} = \frac{mp}{\Delta} . \tag{5}$$

In equation (5), the approximations in equations (2) and (3) have been used, and the result has been generalized to include shearing in either the x_1 or x_2 direction, $\alpha = 1, 2$.

Equations (4a) and (4b) are the standard equations for lateral shearing interferometry found in Murty.[7] Note that as ϵ goes to zero the approximation in equation (5) grows more exact, but at the same time the number of fringes and, therefore, the sensitivity of the system, is decreased. It is important that the grating separation, Δ, and, consequently, the value of ϵ, appropriately balances the competition between maximizing sensitivity and approximating the derivative.

For a transparent material, the phase difference, $\delta S(x_1, x_2)$, in equations (4a) and (4b), is given by the difference in optical path length. As shown by Tippur et.al.[3,4]

$$\delta S(x_1, x_2) \approx \bar{c}h(\hat{\sigma}_{11} + \hat{\sigma}_{22}) , \tag{6}$$

where $\bar{c} = D_1 - \frac{\nu}{E}(n_o - 1)$, D_1 is the stress optic constant, n_o is the index of refraction of the undeformed material, h is the specimen thickness and $\hat{\sigma}_{11}$ and $\hat{\sigma}_{22}$ are plane stress thickness averages of stress components in the material while $\hat{\sigma}_{33} = 0$. Finally substituting (6) into (5) gives the result,

$$\bar{c}h\frac{\partial(\hat{\sigma}_{11} + \hat{\sigma}_{22})}{\partial x_\alpha} \approx \frac{mp}{\Delta}. \tag{7}$$

All interference images produced by the CGS apparatus are interpreted using equation (7). A similar analysis may be carried out for opaque materials in reflection giving results with the same form.[3,4]

For the case of a mixed-mode, K-dominant deformation field at a crack tip,

$$(\hat{\sigma}_{11} + \hat{\sigma}_{22}) = \frac{2}{\sqrt{2\pi r}}(K_I cos\frac{\phi}{2} - K_{II} sin\frac{\phi}{2}), \tag{8}$$

where $r = \sqrt{x_1^2 + x_2^2}$ and $\phi = tan^{-1}(x_2/x_1)$. x_1 and x_2 are the coordinates along the crack length and perpendicular to the crack length, respectively, with the origin at the crack tip. Equation (7) indicates that constructive fringes are formed if

$$A\frac{sin\frac{3}{2}(\phi - \psi)}{\sqrt{2\pi r^3}} = \frac{mp}{\Delta\bar{c}h} \qquad \text{for } x_1 \text{ gradients,} \tag{9a}$$

or

$$A\frac{cos\frac{3}{2}(\phi - \psi)}{\sqrt{2\pi r^3}} = \frac{mp}{\Delta\bar{c}h} \qquad \text{for } x_2 \text{ gradients,} \tag{9b}$$

where $K_I/K_{II} = tan(3\psi/2)$, and $A = K_{II}/cos(3\psi/2)$. An example of the fringe pattern expected from equation (9a) is shown in Figure 4a for $K_{II} = 0$ and Figure 4b for $K_I = 0$. A change in the ratio K_I/K_{II} results in a rotation and/or magnification of the fringe pattern.

3. Experimental Procedure

The specimen geometry is shown in Figure 1a. Specimens are made of PMMA because it approximates the linear elastic assumption of the theoretical solution. Square tip notches $\approx 1.5mm$ thick are cut on a band saw as per the figure. The inclusion of a notch of finite opening rather than a crack allows the generation of a negative mode-I stress field at the notch tip (as long as the notch faces do not come into contact). Thus, the mode-I response of the system can be investigated.

Impact of the specimens is achieved using a Dynatup drop weight tower. The contact area of the drop weight tup is made of steel, and the corners are rounded to reduce stress concentration. The weight is dropped from approximately 1.4 m giving it a velocity of 5.25 m/s at impact. Including the impedance mismatch of the two materials, this results in a contact interface velocity between the specimen and the drop weight of ≈5 m/s.

Set up of the CGS apparatus follows Figure 2. A streak camera is used as the imaging system. The CGS interferograms are generated using an Argon-Ion laser pulsed for 50 ns at 7 μs intervals as the light source. The total length of the test is $\approx$ 300 μs resulting in approximately 40 CGS interferograms per test.

The fringe patterns are digitized by hand. A ray of constant ϕ from the crack tip is followed; points at the center of fringes are digitized along the way. Most of the uncertainty in digitization arises from locating the crack tip and choosing the center of the fringe. Uncertainties in the measurement of ϕ are minimal.

Data is analyzed by rearranging equation (9a) to give

$$\frac{m_i p}{\Delta \bar{c} h} \sqrt{2\pi r_i^3} = Y_i \tag{10}$$

where $Y_i = A sin\frac{3}{2}(\phi_i - \psi)$ and the subscript i refers to individually digitized points. The left hand side of this equation is obviously constant for fixed ϕ, K_I and K_{II}. If K-dominance is exhibited, plotting the left side of equation (10) with respect to r should result in a horizontal line. K-dominance was studied by producing such plots and investigating their slope.

Deviation of experimental results from the fringe patterns predicted by a K-dominant field are expected for various reasons. These include the notch tip geometry, the zone around the notch tip where plane stress assumptions break down (the 3-D zone)[8,9] and the finite specimen size. Once a region of K-dominance is located, however, a "least squares" fitting procedure is performed utilizing only the data from such a region to produce a value for both K_I and K_{II}.

4. Results and Discussion

A series of shearing interferograms is shown in Figure 5. Comparison to Figure 4b shows that the fringes represent a primarily mode II type of deformation at a short time after impact ($c_d t/l \leq 3$). In analogy to observed near-tip three dimensional effects in mode-I deformation[8,9] it is expected that within a radius equal to half the specimen thickness, mixed-mode deformation will have a strongly three dimensional character. As a result, the fringes contained within a radius equal to half the specimen thickness, were always excluded in the analysis. Digitization was always performed outside the 3-D zone for the useable interferograms, and, consequently, the results up to 18μs ($c_d t/l = 1.2$) were rendered un-interpretable.

Before attempting a fit, K-dominance was investigated. The left hand side of equation (10) was plotted for various values of r_i and constant ϕ. Examples of such plots are shown in Figure 6. It can be seen in this figure that in a substantial region surrounding the 3-D zone horizontal lines result. (It is expected that the value of Y_i will depend upon ϕ as seen in the plots.) Thus, K-dominance is a reasonable assumption for data points taken beyond half the thickness from the notch-tip.

Fitting of the theoretical fringes to the digitized points was carried out for a K-dominant field. When the theoretical fringe pattern from the fit has been superimposed on the interferogram from the experiment, it can be seen that the experimental interferogram matches the theoretical fringe pattern quite well. The resulting K values from all the fits are shown in Figure 7 plotted with the analysis of Lee and Freund[1] and the numerical calculations by the same authors.[2] Normalization of the experimental data was achieved using the plane stress values for K', see equation (1). As can be seen, good agreement between the experiment and the analysis is found. In Figure 7a the mode I experimental results follow the numerical simulation closely, but most deviate from the theoretical analysis. This is expected since the theoretical loading has an infinite area of contact while the finite element analysis models our specimen more closely. (In this experiment, the area of contact is small, 1.5 times the crack length; the finite element analysis is carried out for loading area equal to the crack length. This effect also explains the large difference between numerical and analytical predictions.) The good agreement of mode I results indicates that the method is sensitive enough to measure both K_I and K_{II} even when the ratio, K_I/K_{II} is small. In Figure 7b, the mode II results agree well with both the theoretical and numerical analysis.

It is noted that experimentally determining the time of impact i.e. $c_d t/l = 0$ is difficult. Simply watching the tup impact the specimen is not sufficient because in the time between two exposures the tup moves a distance $\approx 1\mu m$. The magnification is ≈ 1; thus, detecting such small motions is impossible. However, at 5 m/s impact velocity, it is possible for the CGS to detect the initial compression wave traveling from the contact area to the crack tip, (see the interferograms in Figure 8) and, thus, determine the time of impact. Measurement of the velocity of this wave ($c_d = 1750$ m/s) agrees well with the expected plane stress velocity in PMMA for a dilatational wave. By extrapolating the wave propagation back to the contact area, the time of impact was found satisfactorily.

In conclusion, the ability of CGS to measure mixed-mode stress intensity factors under dynamic conditions has been examined. The good agreement between experimental results and theory demonstrates that even when mode-mixity is not substantial, the method produces acceptable values for both stress intensity factors.

Acknowledgements

We would like to thank Prof. L.B. Freund and Dr. Y.J. Lee for their many helpful discussions and for making their numerical data available to us prior to publication. We would also like to thank Dr. H. Tippur for his help and advice given in the early stages of this study. Finally, the support of ONR through Contract N00014-90-J-1340 is gratefully acknowledged.

References

1. Y.J. Lee and L.B. Freund,"Fracture Initiation Due to Asymmetric Impact Loading of and Edge Cracked Plate," Journal of Applied Mechanics, v. 57, pp. 104-111, 1990

2. Y.J. Lee and L.B. Freund, Private Communication, 1990

3. H.V. Tippur, S. Krishnaswamy and A.J. Rosakis, "A Coherent Gradient Sensor for Crack Tip Deformation Measurements: Analysis and Experimental Results," International Journal of Fracture, v. 48, pp. 193-204, 1991

4. H.V. Tippur, S. Krishnaswamy and A.J. Rosakis, "Optical Mapping of Crack Tip Deformations Using the Methods of Transmission and Reflection Coherent Gradient Sensing," Caltech Report SM89-11, (submitted to International Journal of Fracture) 1989

5. P. Hariharan, W.H. Steel and J.C. Wyant, "Double Grating Interferometer with Variable Lateral Shear," Optics Communications, v. 11, no. 3, pp. 317-320, 1974

6. P. Hariharan and Z.S. Hegedus, "Double Grating Interferometers II. Application to Collimated Beams," Optics Communications, v. 14, no. 1, pp. 148-151, 1975

7. M.V.R.K. Murty, "Lateral Shearing Interferometers," Optical Shop Testing, D. Malacara, Ed., J. Wiley & Sons, New York, 1978

8. A.J. Rosakis and K. Ravi-Chandar, "On Crack-Tip Stress State: An Experimental Evaluation of Three-Dimensional Effects," International Journal of Solids & Structures, vol. 22, no. 2, p. 121-134, 1986

9. S. Krishnaswamy, A.J. Rosakis and G. Ravichandran, "On the Extent of Dominance of Asymptotic Elastodynamic Crack Tip Fields; Part II: Numerical Investigation of Three-Dimensional and Transient Effects," Caltech Report SM88-22, (submitted to Journal of Applied Mechanics), 1988

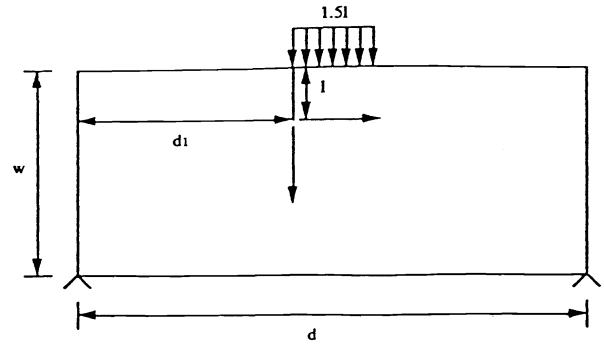

(a)

Dimensions of specimen :
l=25mm
w=127mm
d=254mm
d_1=136mm
thickness=7.5mm

Mechanical properties of specimen:
E=1240 MPa
v=0.35
c=1.08 10^{-10} Pa
$c_d^{pl-\sigma}$=1765 m/s

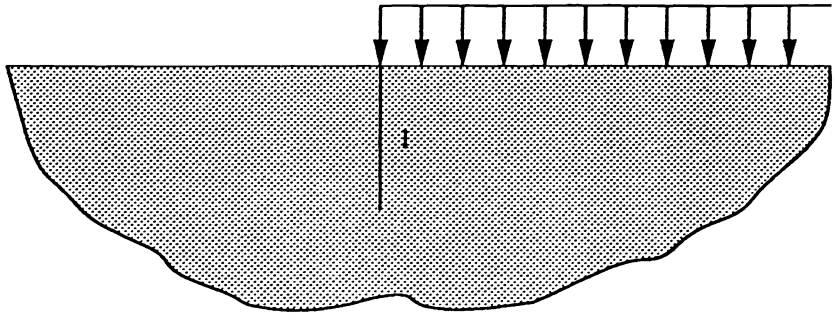

(b)

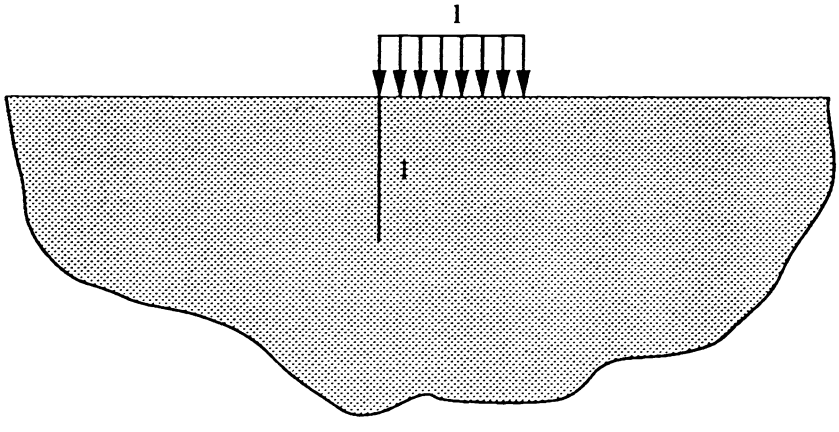

(c)

FIGURE 1 : Loading configuration and geometry for (a) present experimental study, (b) Theoretical solution by Lee and Freund [1] and (c) finite element simulation of Lee and Freund [2]

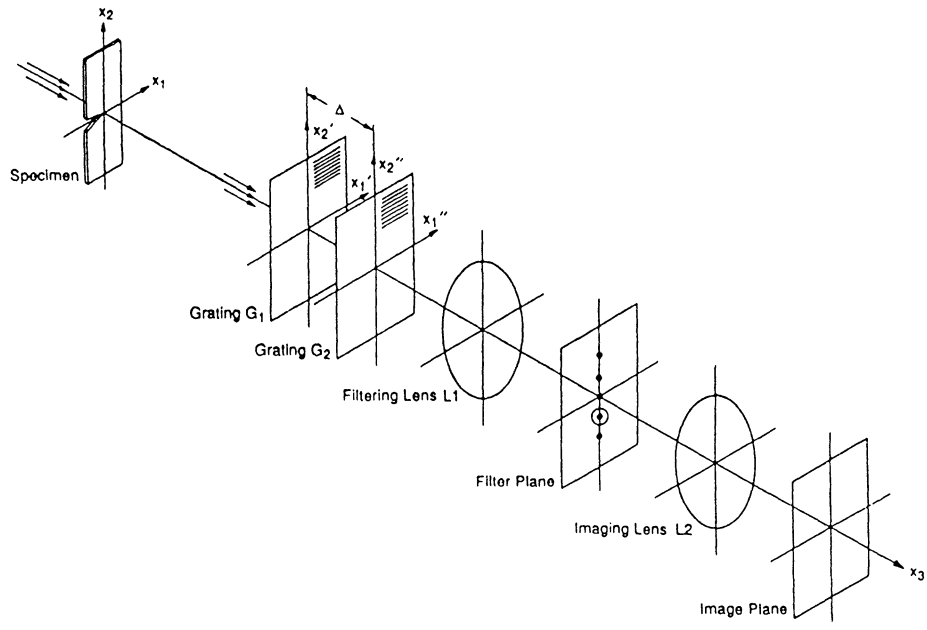

FIGURE 2 : Schematic of the experimental set-up for transmission CGS.

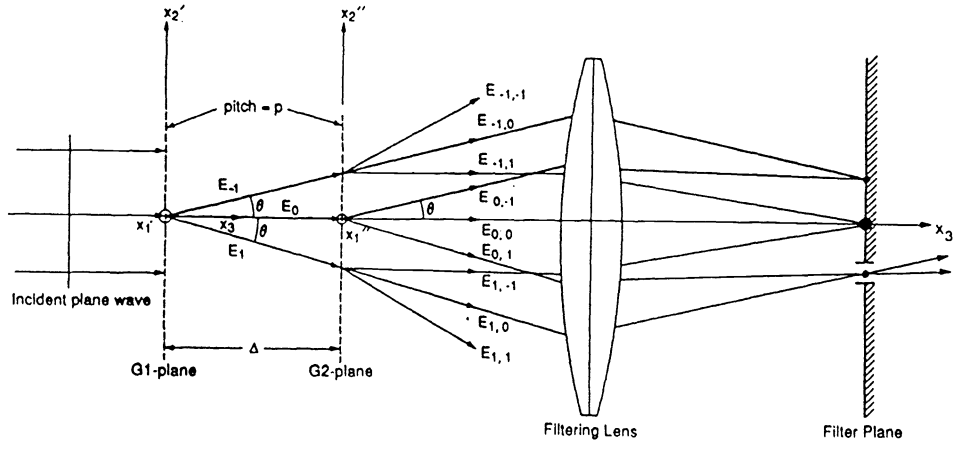

FIGURE 3 : Schematic describing the working principle of CGS.

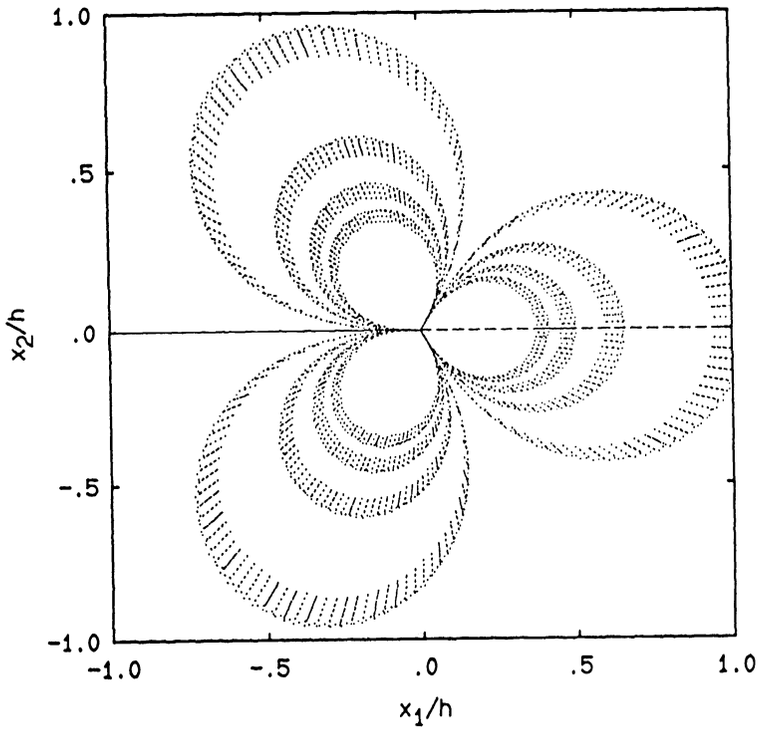

FIGURE 4 (a) : Numerical predictions of CGS fringes (constant $\partial(\sigma_{11}+\sigma_{22})/\partial x_1$ values) constructed on the basis of a pure K_I field.

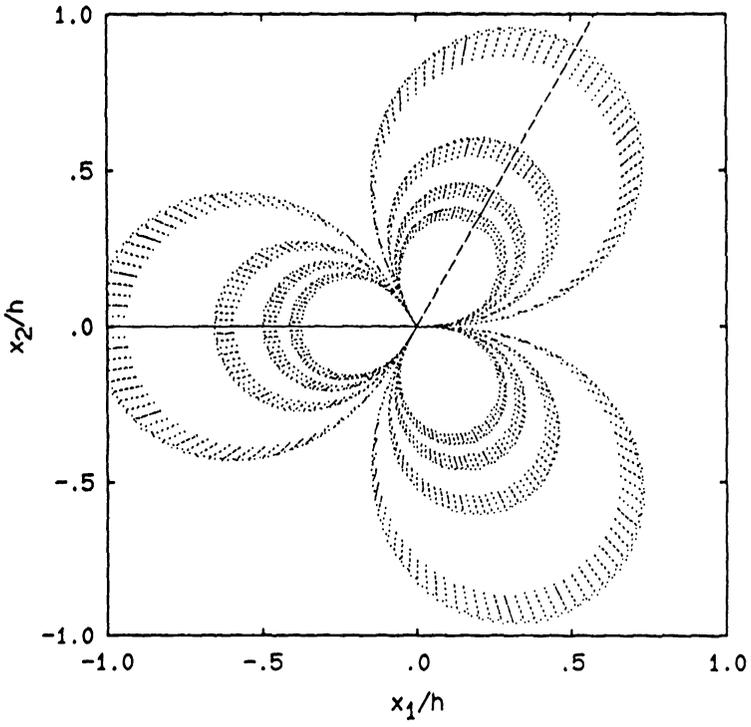

FIGURE 4 (b) : Numerical predictions of CGS fringes (constant $\partial(\sigma_{11}+\sigma_{22})/\partial x_1$ values) constructed on the basis of a pure K_{II} field.

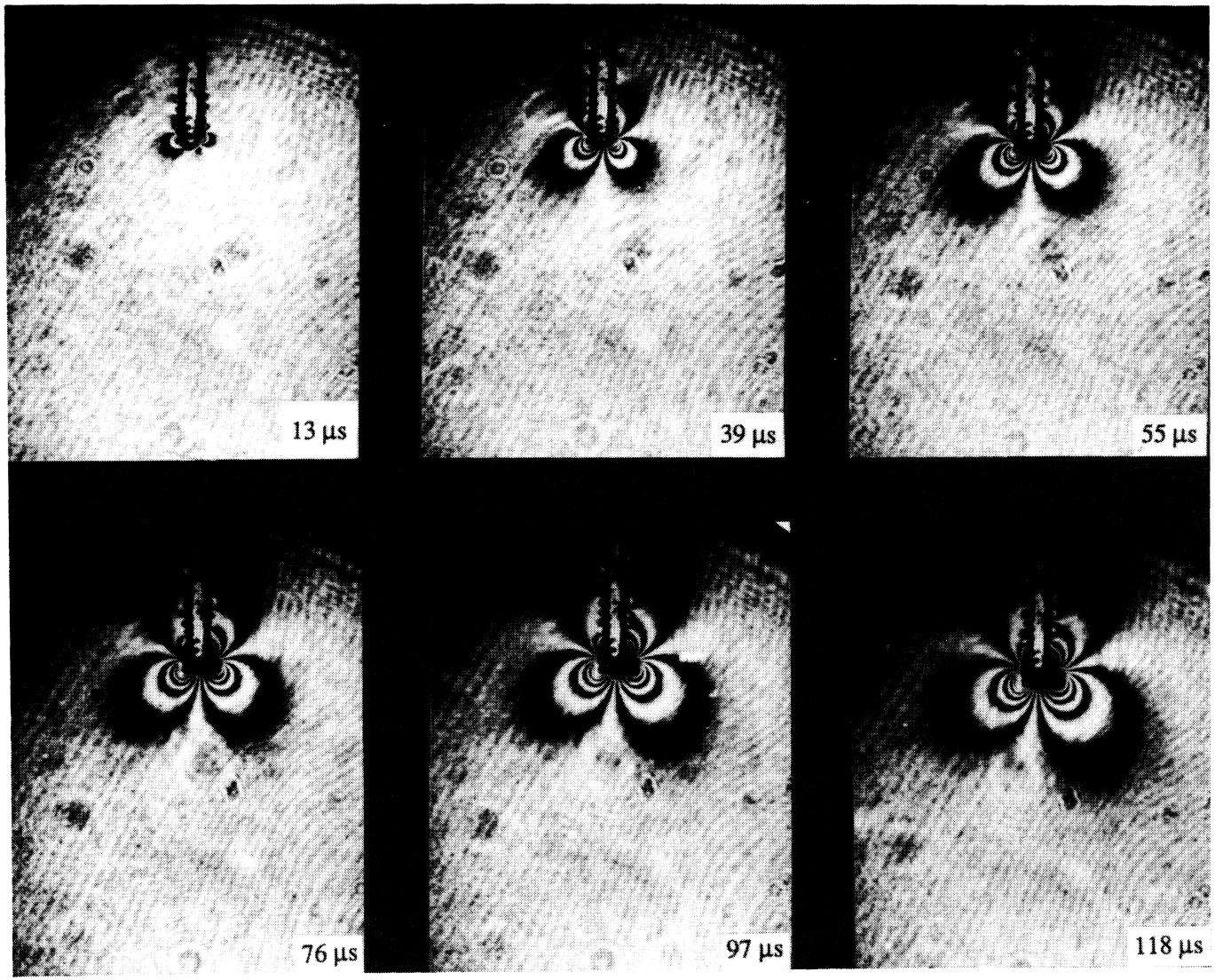

FIGURE 5 : Sequence of CGS interferograms corresponding to initial stages of the dynamic asymmetric loading of the prenotched specimen.

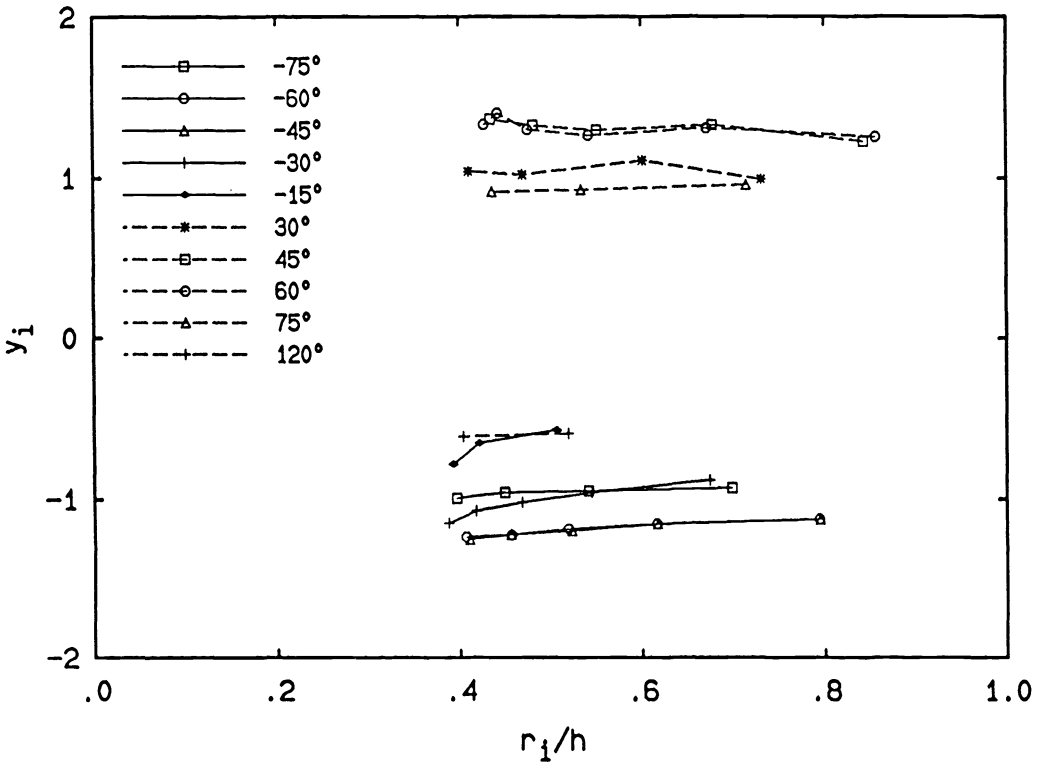

FIGURE 6 : Radial variation of y_i for various ϕ at a time t=49μs ($c_d t/l$ =3.3) after impact.

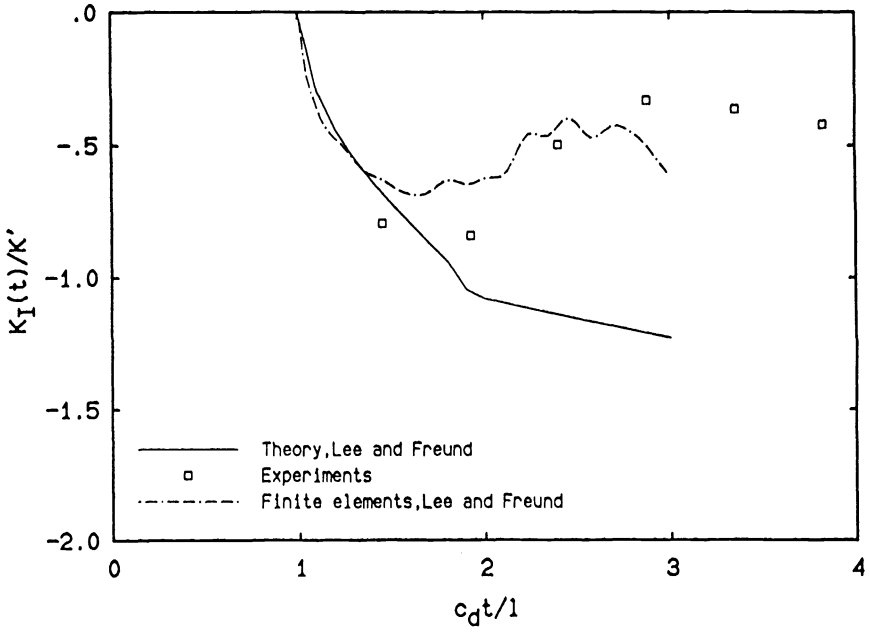

FIGURE 7 (a) : Normalised stress intensity factor as a function of normalized time, for "short" times,$c_d t/l<3$ Comparison of theoretical analysis of Lee and Freund [1], numerical analysis of Lee and Freund [2]and experimental results for mode I.

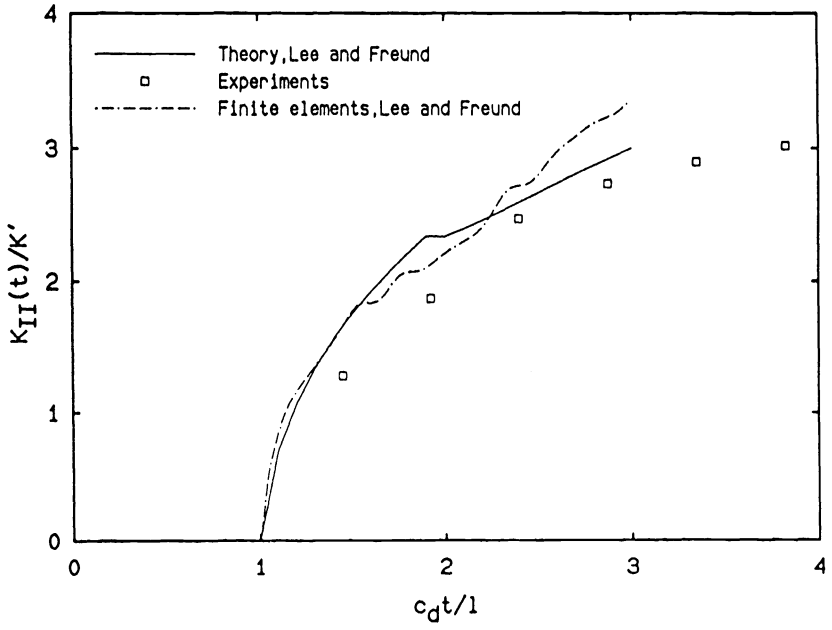

FIGURE 7 (b) : Normalized stress intensity factor as a function of normalized time, for "short" times,$c_d t/l<3$. Comparison of theoretical analysis of Lee and Freund [1], numerical analysis of Lee and Freund [2] and experimental results for mode II.

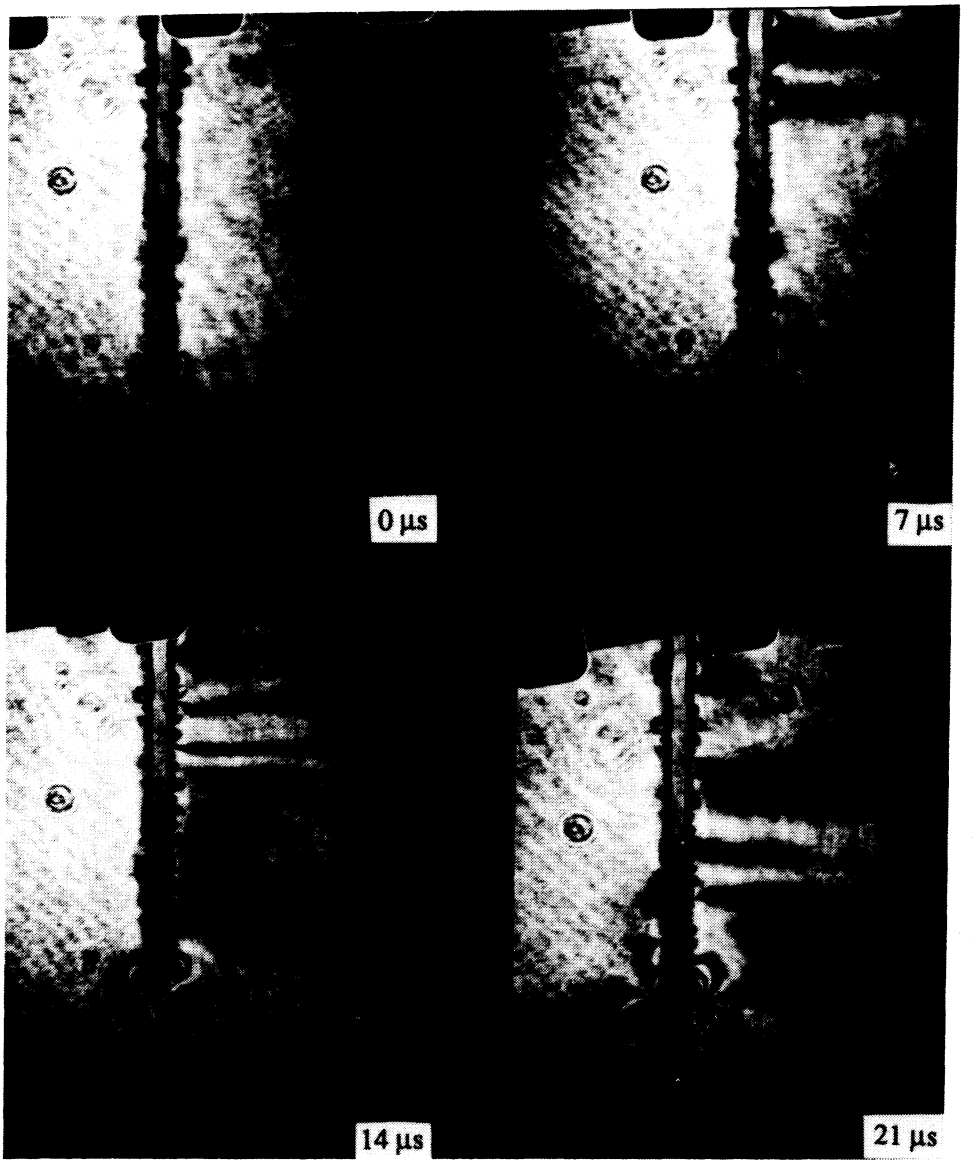

FIGURE 8 : A sequence of high speed images showing compressive waves generated during impact approaching the notch tip